

Coexistence of ferromagnetism and superconductivity at KTaO_3 heterointerfaces

Zhongfeng Ning,¹ Jiahui Qian,¹ Yixin Liu,^{2,3} Fan Chen,^{2,3} Mingzhu Zhang,^{2,3} Liwei Deng,^{2,3} Xinli Yuan,⁴ Qingqin Ge,⁴ Hua Jin,² Guanqun Zhang,¹ Wei Peng,^{2,3} Shan Qiao,^{2,3,*} Gang Mu,^{2,3,*} Yan Chen^{1,*} and Wei Li^{1,*}

¹State Key Laboratory of Surface Physics and Department of Physics, Fudan University, Shanghai 200433, China

²National Key Laboratory of Materials for Integrated Circuits,
Shanghai Institute of Microsystem and Information Technology,
Chinese Academy of Sciences, Shanghai 200050, China

³University of Chinese Academy of Sciences, Beijing 100049, China

⁴Thermo Fisher Scientific China, Shanghai 201203, China

(Dated: May 31, 2024)

ABSTRACT: The coexistence of superconductivity and ferromagnetism is a long-standing issue in superconductivity due to the antagonistic nature of these two ordered states. Experimentally identifying and characterizing novel heterointerface superconductors that coexist with magnetism presents significant challenges. Here, we report the experimental observation of two-dimensional long-range ferromagnetic order in the KTaO_3 heterointerface superconductor, showing the coexistence of superconductivity and ferromagnetism. Remarkably, our direct current superconducting quantum interference device measurements reveal an in-plane magnetization hysteresis loop persisting above room temperature. Moreover, the first-principles calculations and X-ray magnetic circular dichroism measurements provide decisive insights into the origin of the observed robust ferromagnetism, attributing it to oxygen vacancies that localize electrons in nearby Ta $5d$ states. Our findings not only suggest KTaO_3 heterointerfaces as time-reversal symmetry breaking superconductors, but also inject fresh momentum into the exploration of the intricate interplay between superconductivity and magnetism, enhanced by the strong spin-orbit coupling inherent to the heavy Ta in $5d$ orbitals of KTaO_3 heterointerfaces.

Keywords: heterointerface, two dimensions, superconductivity, ferromagnetism, spin-orbit coupling

INTRODUCTION

Two-dimensional oxide heterointerfaces exhibit a wide range of emergent quantum phenomena inaccessible in their bulk individuals due to the strong interplay between electrons with Coulomb interaction and the interfacial electron-phonon coupling at the interfaces¹⁻³. Among them, a landmark oxide interface is $\text{LaAlO}_3/\text{SrTiO}_3$ ⁴, which displays a plethora of appealing physical properties, encompassing two-dimensional electron gases with high electron mobility⁵, strong Rashba-like spin-orbit coupling⁶⁻⁸, interfacial superconductivity^{9,10}, and ferromagnetism^{11,12}. In particular, the coexistence of superconductivity and ferromagnetism has also been unveiled by high-resolution magnetic torque magnetometry¹³, scanning superconducting quantum interference device (SQUID)¹⁴, and magnetoresistance¹⁵. This suggests the presence of a nontrivial superconducting phase in the ground state, such as an intriguing Fulde-Ferrell-Larkin-Ovchinnikov-type condensate of Cooper pairs with finite momentum¹⁶ and a mixed-parity superconducting phase with an admixture of spin-singlet and spin-triplet pairing components^{17,18} that is a candidate platform for realizing Majorana modes¹⁹. However, the experimental challenges posed by the extremely low superconducting critical temperature T_c (below 250 mK) of SrTiO_3 heterointerfaces have hindered a comprehensive exploration of the underlying properties⁹, leaving the origin of these quantum phases still elusive^{20,21} and motivating the search for a more favorable heterointerface superconductor that hosts the intricate interplay between ferromagnetism and superconductivity.

Very recently, an unforeseen crystalline-orientation-dependent superconductivity has been observed at KTaO_3 heterointerfaces with T_c as high as 2 K²²⁻²⁵. This is nearly one order of magnitude higher in T_c than that of SrTiO_3 ⁹. The experimental findings also demonstrate that electronic states near the Fermi energy derived from Ta $5d$ orbitals with strong spin-orbit coupling play a decisive role in electronic conduction at the KTaO_3 heterointerfaces²⁶⁻³⁰. Moreover, the existence of intrinsic anomalous Hall effect observed by electrical transport measurements at non-superconducting KTaO_3 heterointerfaces^{31,32} suggests an emergent ferromagnetism with time-reversal symmetry breaking. Additionally, at superconducting KTaO_3 heterointerfaces, the in-plane azimuthal angle-dependent magnetoresistance and the superconducting critical field exhibit striking twofold symmetric oscillations deep inside the superconducting phase, whereas the anisotropy vanishes in the normal phase, as highlighted in our recent notable study²⁴. This observation indicates the intrinsic nature of the mixed-parity superconducting ground state with an admixture of s -wave and p -wave pairing components inherent to the inversion symmetry breaking at the KTaO_3 heterointerfaces²⁴. Although the component of p -wave pairing could be theoretically stabilized by the long-range ferromagnetic order^{33,34}, the existence of ferromagnetism at superconducting KTaO_3 heterointerfaces, akin to the observation at superconducting SrTiO_3 heterointerfaces¹³⁻¹⁵, is highly desired to examine by using direct experimental accesses.

In this work, utilizing the measurements of direct cur-

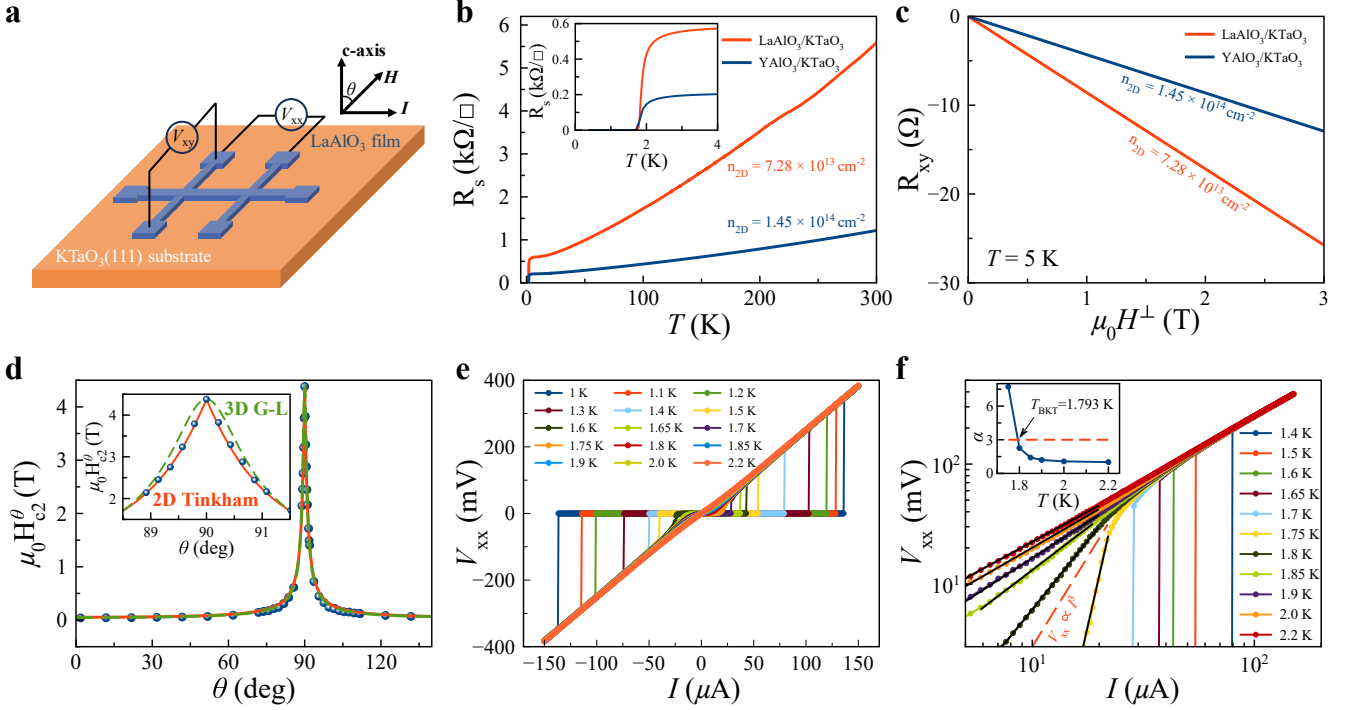


FIG. 1. Two-dimensional superconductivity of KTaO₃ heterointerfaces. (a) Schematic structure of the Hall bar device on a representative LaAlO₃/KTaO₃(111). (b) Longitudinal electrical resistance R_s as a function of temperature for LaAlO₃ and YAlO₃ films on KTaO₃(111) substrates. Inset: Magnified view of the low temperature regime. (c) Corresponding perpendicular field $\mu_0 H^\perp$ -dependent transverse Hall resistance R_{xy} measured at the temperature of 5 K. (d) Out-of-plane polar angular θ dependence of $\mu_0 H_{c2}^\theta$ for LaAlO₃/KTaO₃(111). Inset: Magnified view around $\theta = 90^\circ$. The red solid and green dotted lines represent theoretical fits using the two-dimensional (2D) Tinkham and the three-dimensional (3D) anisotropic Ginzburg-Landau (G-L) models, respectively. (e) Temperature-dependent I - V_{xx} measurements for LaAlO₃/KTaO₃(111). (f) Corresponding logarithmic scale representation of (e). The red dashed line indicates $V_{xx} \propto I^3$. Inset: The extracted power-law fitting exponent α as a function of T . The $T_{\text{BKT}} = 1.793$ K is defined by $\alpha = 3$.

rent SQUID, we observe a distinct signal of an in-plane ferromagnetic hysteresis loop in the KTaO₃ heterointerface superconductor, attributing it to intrinsic ferromagnetism that persists above room temperature. Moreover, the first-principles calculations and X-ray magnetic circular dichroism (XMCD) measurements provide decisive evidences in support of the robust ferromagnetism of superconducting KTaO₃ heterointerfaces, which derives from the local moments of the Ta⁴⁺: $5d^1$ ions brought about by the oxygen vacancies that host the two-dimensional electron gases formed at the KTaO₃ heterointerfaces, which are responsible for the emergence of interfacial superconductivity. Remarkably, these findings indicate the coexistence of ferromagnetism and superconductivity at the KTaO₃ heterointerfaces, offering novel insights into the intricate superconducting properties at these interfaces.

RESULTS AND DISCUSSION

Both the LaAlO₃ and YAlO₃ thin films are grown by pulsed laser deposition on top of the single-crystalline KTaO₃(111) substrates (see Methods in Supporting Information). Atomic force microscopy (AFM) characterization reveals that the surface of KTaO₃ substrates and thin films are atomically flat (see Figure S1, YAlO₃

shown in Ref. 24), suggesting a high-quality growth of the thin films on KTaO₃. On the other hand, X-ray diffraction (XRD) exposes the absence of epitaxial Bragg reflection peaks in both the LaAlO₃ and YAlO₃ thin films (see Figure S2, YAlO₃ presented in Ref. 24), confirming the deposition of an amorphous phase for both the LaAlO₃ and YAlO₃ thin films on the KTaO₃(111) substrates. These results align well with previous investigations^{22–24}. Subsequently, we conduct electrical transport measurements on the devices of the as-grown thin films arranged in Hall bar configurations (see Figure 1a)^{24,35}.

The longitudinal electrical resistances R_s in Figure 1b exhibit metallic behavior from room temperature to 2.5 K for both LaAlO₃/KTaO₃(111) and YAlO₃/KTaO₃(111), indicating the formation of two-dimensional electron gases at their heterointerfaces, given that their bulk constituents are nonmagnetic insulators. In addition, the charge carriers in both cases are electrons with an estimated charge carrier density of $7.28 \times 10^{13} \text{ cm}^{-2}$ and $1.45 \times 10^{14} \text{ cm}^{-2}$, respectively, by the Hall measurements at 5 K (see Figure 1c). Remarkably, the superconducting transitions start at $T_c^{\text{onset}} = 2.32$ K and 2.39 K, and resistances drop to zero at $T_c^{\text{zero}} = 1.66$ K and 1.7 K, respectively, for LaAlO₃/KTaO₃ and YAlO₃/KTaO₃. In the LaAlO₃/KTaO₃(111), the field-dependent R_s shown in

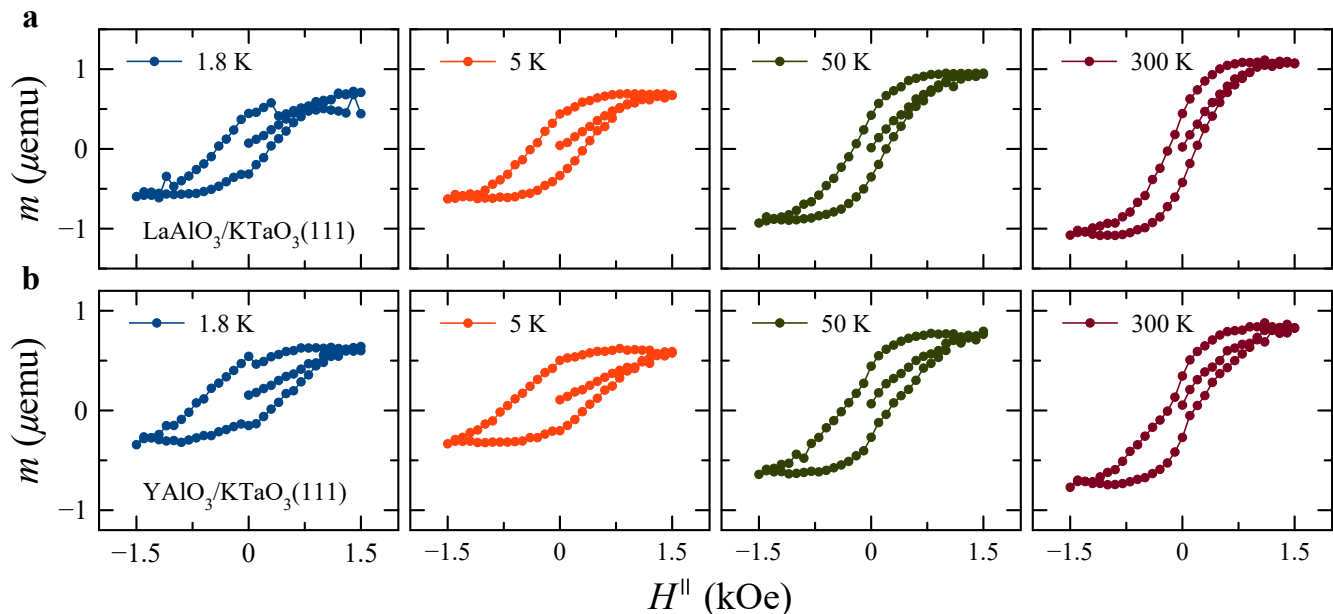


FIG. 2. Ferromagnetic properties of KTaO₃ heterointerfaces. Temperature-dependent in-plane ferromagnetic hysteresis loops (m - H^{\parallel}) for (a) LaAlO₃/KTaO₃(111) and (b) YAlO₃/KTaO₃(111), corrected for the diamagnetic contribution of the bare KTaO₃ substrate. The applied magnetic field H^{\parallel} ranges from -1.5 kOe to +1.5 kOe, with the field parallel to the surface of thin films.

Figure S3 yields the upper critical fields $\mu_0 H_{c2}^{\parallel}(0.6 \text{ K}) = 5 \text{ T}$ for fields parallel to the sample plane surface and $\mu_0 H_{c2}^{\perp}(0.6 \text{ K}) = 0.45 \text{ T}$ for fields parallel to the crystallographic c -axis. Here, $\mu_0 H_{c2}$ is defined as the magnetic field at the midpoint of the electrical resistance transition. The extracted temperature dependence of $\mu_0 H_{c2}$ is shown in Figure S3c, where a large ratio $H_{c2}^{\parallel}/H_{c2}^{\perp}$ is perceived, suggesting strong anisotropic superconductivity of LaAlO₃/KTaO₃(111). Quantitatively, the out-of-plane polar angular θ -dependent $\mu_0 H_{c2}^{\theta}$ at 1.6 K is used to verify this intriguing behavior, as shown in Figure 1d. Using the two-dimensional Tinkham and the three-dimensional anisotropic Ginzburg-Landau models to fit the $\mu_0 H_{c2}^{\theta}$, given by $\frac{H_{c2}^{\theta} |\cos \theta|}{H_{c2}^{\parallel}} + \left(\frac{H_{c2}^{\theta} \sin \theta}{H_{c2}^{\perp}}\right)^2 = 1$ and $\left(\frac{H_{c2}^{\theta} \cos \theta}{H_{c2}^{\parallel}}\right)^2 + \left(\frac{H_{c2}^{\theta} \sin \theta}{H_{c2}^{\perp}}\right)^2 = 1$, respectively^{36,37}, a cusp-like peak is clearly observed at around $\theta = 90^\circ$ (see Figure 1d, inset), which is well described by the two-dimensional Tinkham model, as frequently observed in heterointerface superconductivity^{24,37,38} and layered transition metal dichalcogenides^{33,39}. Qualitatively similar results have also been observed in YAlO₃/KTaO₃²⁴, unambiguously demonstrating the intrinsic two-dimensional superconductivity at the KTaO₃ heterointerfaces.

To further examine the intrinsic interfacial superconductivity at the KTaO₃ heterointerfaces, we conduct measurements of the current-voltage (I - V_{xx}) characteristics at various temperatures near T_c (see Figure 1e). These characteristics, depicted on a log-log scale in Figure 1f, reveal a distinct critical current I_c of 79.1 μA at 1.4 K, below T_c . The I_c gradually decreases with increas-

ing T , eventually vanishing, indicating a transition from superconducting to normal phases. In the normal phase, we have $V_{xx} \propto I$ according to Ohm's law. However, a steeper power law $V_{xx} \propto I^{\alpha(T)}$ emerges as T drops. Following the Berezinskii-Kosterlitz-Thouless (BKT) definition^{40,41}, the transition temperature T_{BKT} corresponds to the dissociation of vortex-antivortex pairs. This obeys the universal scaling relation $V_{xx} \propto I^3$, since the superconducting phase consists of bound vortex-antivortex pairs in two-dimensional superconductors. We determine $T_{\text{BKT}} = 1.793 \text{ K}$ from where $\alpha = 3$ interpolates. Furthermore, T_{BKT} can be alternatively evaluated from the formula $R_s = R_0 \exp[-b(T/T_{\text{BKT}} - 1)^{-1/2}]$, where R_0 and b are material parameters⁴². Applying such a theoretical fit to the measured R_s yields $T_{\text{BKT}} = 1.878 \text{ K}$ (see Figure S4). As expected, the T_{BKT} obtained from these two independent approaches is close to T_c^{zero} , providing additional evidence for the two-dimensional superconducting nature of the KTaO₃ heterointerfaces.

Next, we delve into the magnetic properties of KTaO₃ heterointerfaces. Theoretically, the two-dimensional conducting electron gases at the interfaces of KTaO₃ heterostructures primarily originate from the partially filled $5d$ orbitals of the Ta atoms induced by oxygen vacancies^{23,24}, these vacancies themselves have the potential to induce ferromagnetism. Experimentally, the zero-field-cooling (ZFC) and field-cooling (FC) curves of the as-grown thin films of LaAlO₃ and YAlO₃, measured at a temperature between 1.8 and 300 K with an applied in-plane field (H^{\parallel}) of 50 Oe, are summarized in Figure S5. The figures exhibit the pronounced separation between the ZFC and FC curves up to 300 K, showing a sig-

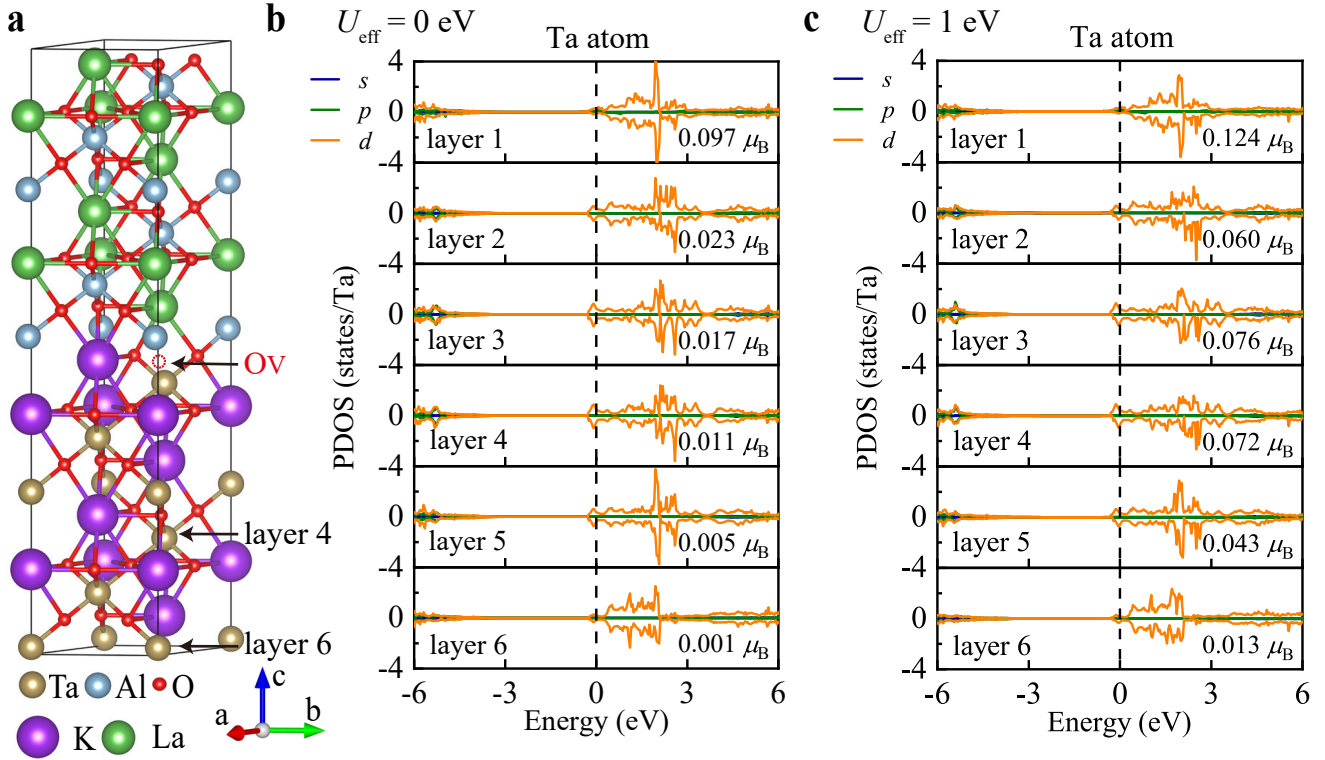


FIG. 3. First-principles calculations on the KTaO₃ heterointerface. (a) Schematic structure of the superlattices (LaAlO₃)₆/(KTaO₃)₆(111) with the presence of an oxygen vacancy. The red dotted circle denotes the oxygen vacancy (O_V) at the heterointerface of LaAlO₃/KTaO₃(111). The PDOS for Ta atoms, calculated by using the GGA+ U_{eff} method with (b) $U_{\text{eff}} = 0$ eV and (c) $U_{\text{eff}} = 1.0$ eV. The numbers listed in the figure represent the magnetization of Ta in each layer. Here, we set the Fermi energy to zero.

nature of in-plane ferromagnetism at the superconducting KTaO₃ heterointerfaces that persists at room temperature. In Figure 2, the well-defined magnetization-magnetic field ($m \sim H^{\parallel}$) hysteresis loops observed at different temperatures for the LaAlO₃/KTaO₃ and YAlO₃/KTaO₃ provide clear evidence of the temperature dependence of long-range ferromagnetic order. Control experiments on an as-received KTaO₃ substrate without LaAlO₃ or YAlO₃ overlayers only show a diamagnetic background (see Figures S6 and S7). Additionally, we conduct X-ray photoelectron spectroscopy (XPS) and scanning electron microscopy (SEM)-energy dispersive X-ray spectroscopy (EDS) measurements to actively eliminate concerns related to extrinsic magnetic contamination during sample preparation. As anticipated, the samples exhibit no evidence of magnetic elements, such as Fe, Co, Mn, Ni or Cr, as shown in Figures S8 and S9. As a consequence, we attribute the universally and consistently observed distinct ferromagnetic signal depicted in Figure 2 to the intrinsic nature of the KTaO₃ heterointerfaces. Specifically, we attribute the emergence of two-dimensional ferromagnetism to the Ta⁴⁺ : 5d¹ electrons induced by the high concentration of oxygen vacancies at the KTaO₃ heterointerfaces²³. This observation is noteworthy because their bulk counterparts are typical nonmagnetic insulators. It is also important to note that

the distinction contrasts with a previous report, in which the ferromagnetic response originates from an extrinsic magnetic thin film of EuO^{43,44}.

Furthermore, we actively compare the in-plane and out-of-plane $m \sim H$ loop SQUID measurements of the LaAlO₃/KTaO₃ and YAlO₃/KTaO₃ (see Figures S10-S13). These measurements indicate that the temperature dependence of the long-range ferromagnetic order aligns with the in-plane orientation of the KTaO₃ heterointerfaces, a consistency observed with the results from the first-principles calculations (see also the first-principles calculations below for a comprehensive analysis) and the anomalous Hall effect and the in-plane field-dependent magnetoresistance with butterfly-like hysteresis (see Figure S14). In addition, we quantify the in-plane magnetization of the itinerant electron gases formed at the KTaO₃ heterointerfaces, revealing a magnitude of approximately $\simeq 0.2 \mu_B$ per interface unit cell (if we attribute all the magnetization to the interface). It is interesting to indicate that the KTaO₃ heterointerfaces display a non-monotonic behavior in temperature-dependent magnetization (see Figure 2 and Figure S15). This non-monotonic pattern, also observed in previously explored LaAlO₃/SrTiO₃¹² and VSe₂ monolayers on van der Waals substrates⁴⁵, is attributed to the structural phase and charge-density-wave

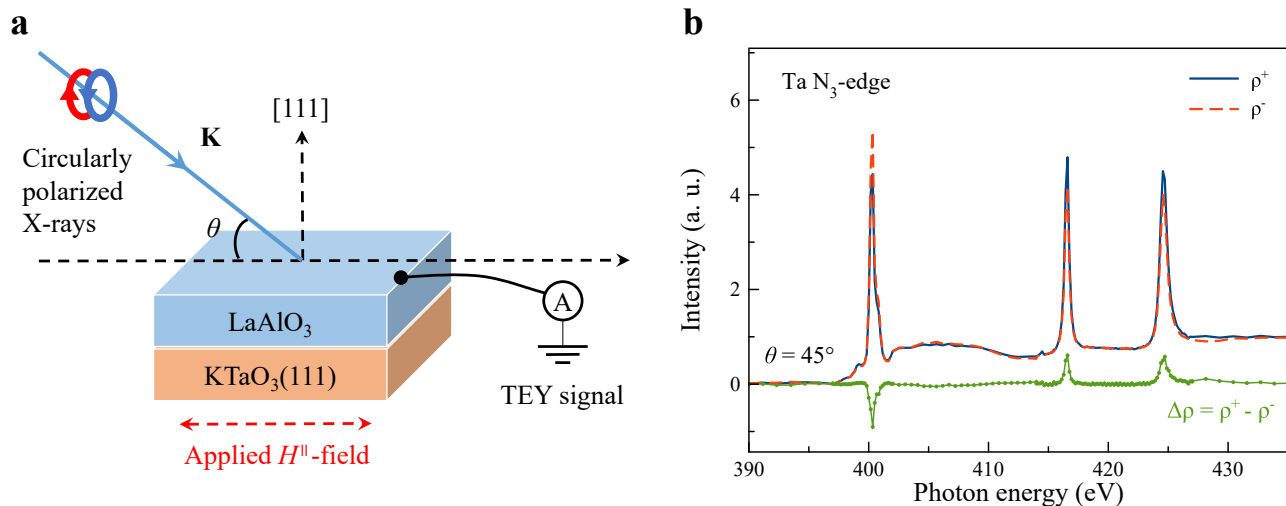


FIG. 4. XMCD measurement on a $\text{LaAlO}_3/\text{KTaO}_3(111)$ heterostructure. (a) Schematic illustration of the experimental configuration for the XMCD measurement, where \mathbf{K} represents the x-ray propagation vector. (b) Spectrum of the XMCD at Ta N_3 absorption edge observed in the in-plane geometry with a fixed incidence angle $\theta = 45^\circ$, revealing ferromagnetic Ta at $T = 15$ K.

transitions, respectively. Since KTaO_3 shares a number of properties in common with SrTiO_3 ²⁴, the observed non-monotonic temperature-dependent magnetization at KTaO_3 heterointerfaces may be also attributed to the structural phase transitions located at the heterointerfaces. This non-monotonicity underscores the critical role of the KTaO_3 surface and its phase transition in the origin of these emergent magnetic properties, and LaAlO_3 or YAlO_3 overlayers significantly amplify these effects by forming two-dimensional electron gases at the KTaO_3 heterointerfaces¹². Further experimental efforts would be needed to confirm this underlying nature of the observed non-monotonicity in temperature-dependent magnetization. Moreover, at the lowest temperature of this measurement limited $T = 1.8$ K, which is also lower than T_c^{onset} [2.32 K for $\text{LaAlO}_3/\text{KTaO}_3(111)$ and 2.39 K for $\text{YAlO}_3/\text{KTaO}_3(111)$], the conspicuous signal of in-plane ferromagnetic hysteresis loops is reproducibly observed in the superconducting transition regime (see Figure 2), and the magnetization does not seem to be expelled entirely below T_c . These universal and striking results are strongly reminiscent of the superconducting KTaO_3 heterointerfaces spatially coexisting ferromagnetic order⁴⁶ (see also Figure S14). Therefore, we experimentally suggest the coexistence of ferromagnetism and superconductivity at the KTaO_3 heterointerfaces, which has also long been a topic of interest sought in nanoscience and nanotechnology communities⁴⁷.

To deepen our understanding of the intrinsic ferromagnetism emerging at the KTaO_3 heterointerfaces, we delve into the electronic and magnetic properties using the first-principles calculations (see Methods in Supporting Information). For simplicity, we establish a theoretical model with the superlattice $(\text{KTaO}_3)_6/(\text{LaAlO}_3)_6(111)$ comprising a supercell of six

layers each for LaAlO_3 and KTaO_3 , despite the amorphous phase of LaAlO_3 thin films grown on $\text{KTaO}_3(111)$ substrates (see Figure S2), as schematically illustrated in Figure S16a. Interestingly, in the stoichiometric heterostructure $(\text{KTaO}_3)_6/(\text{LaAlO}_3)_6(111)$, devoid of oxygen vacancy, the calculated layer-dependent projected density-of-states (PDOS) reveal that the system is a non-magnetic band insulator with an energy band gap of $\simeq 3.0$ eV (see Figure S16), consistent with previous studies⁴⁸. This result indicates that the emergent two-dimensional electron gases at the KTaO_3 heterointerfaces are unlikely to stem from the diverging Coulomb field due to the polarity of individual layers of LaAlO_3 and KTaO_3 , but rather from the presence of oxygen vacancies.

Principally, each oxygen vacancy donates two electrons into the $\text{LaAlO}_3/\text{KTaO}_3(111)$ interface. In turn, the induced interface charges are typically spread over adjacent layers, giving rise to a $\text{Ta}^{4+}\sim\text{O}^{2-}\sim\text{Ta}^{5+}$ -like electronic configuration, which corresponds to several partially filled Ta $5d$ sub-bands that can lead to interfacial ferromagnetism. As expected, density functional theory calculations show that in the presence of oxygen vacancies (O_V , denoted by red dotted circle shown in Figure 3a), the system behaves as a ferromagnetic metal with the conducting electrons mainly derived from the Ta $5d$ orbitals partially hybridized with the oxygen $2p$ orbitals (see Figure S17), which are responsible for the emergence of two-dimensional superconductivity^{22,26}. Furthermore, Figure 3b,c show the spin-resolved PDOS for Ta atoms associated with the value of the magnetic moments of each Ta layer. The calculated magnetic moment of Ta, brought about by the nearby oxygen vacancy, is about $0.124 \mu_B$ (see Figure 3c). These calculated results align qualitatively and quantitatively with the magnetization measurements presented in Figure 2,

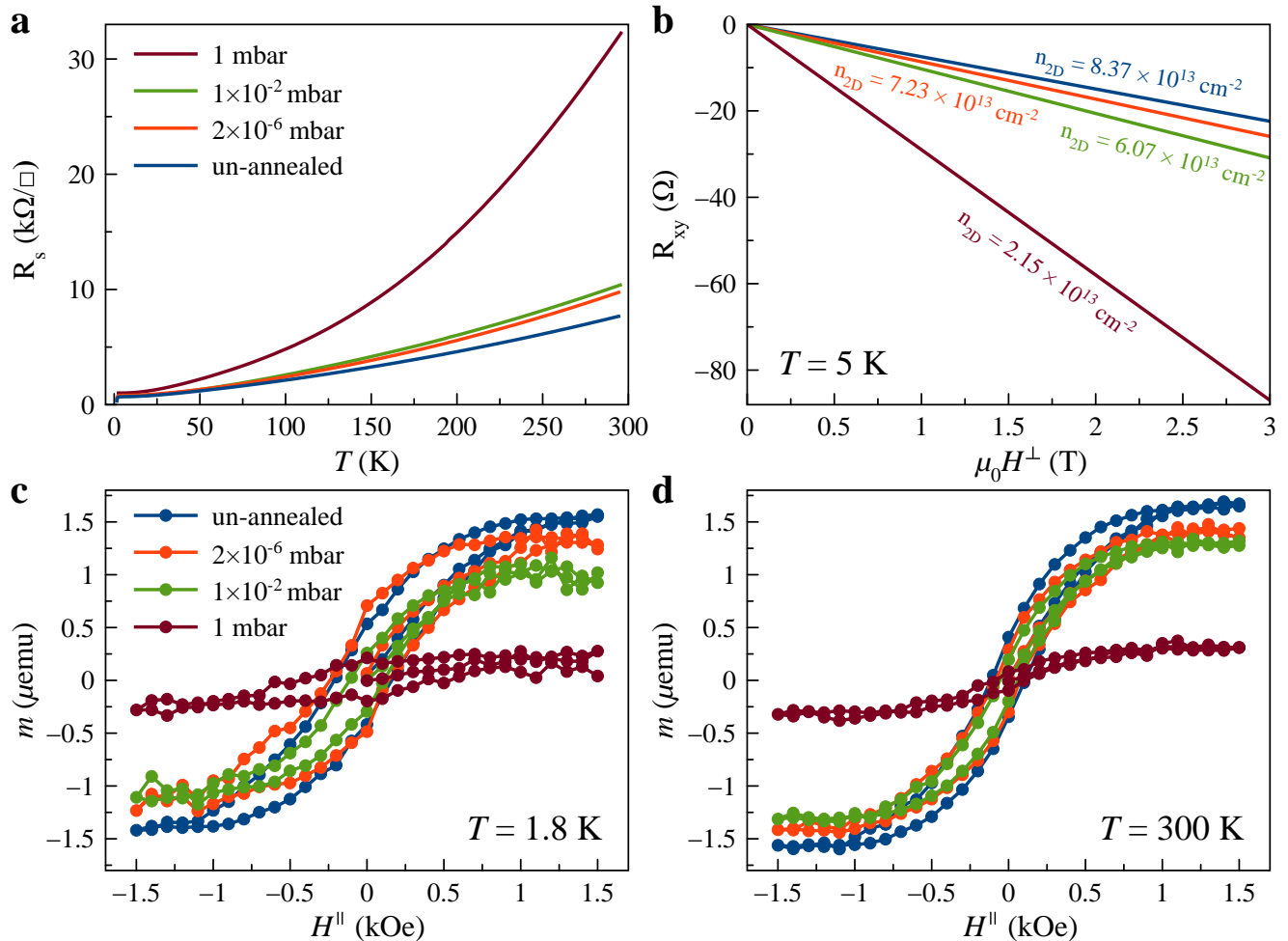


FIG. 5. Influence of post-annealing processes. (a) R_s as a function of T for $\text{LaAlO}_3/\text{KTaO}_3(111)$ subjected to post-annealing processes in various oxygen partial pressures of 1, 1×10^{-2} , and 2×10^{-6} mbar at 400°C for 1 h. We also include the data from the un-annealed $\text{LaAlO}_3/\text{KTaO}_3(111)$ sample. (b) Corresponding transverse Hall resistance R_{xy} as a function of $\mu_0 H^\perp$ at 5 K. In-plane magnetization measured at (c) 1.8 K and (d) 300 K for films subjected to post-annealing processes. It is important to note that the diamagnetic background from the KTaO_3 substrate has been subtracted on the high field slope at each measured temperature.

affirming the intrinsic nature of the long-range ferromagnetic order at the KTaO_3 heterointerface. Additionally, it is noteworthy that we have adjusted the electron correlation effect of Ta $5d$ orbitals through the simplified on-site repulsion strength U_{eff} on Ta $5d$ orbitals⁴⁹. This adjustment yields a magnetic moment that closely corresponds to the experimental findings (see Figure 3c and Figure S18).

Experimentally, we independently conduct synchrotron XMCD measurements (see Methods in Supporting Information) to further investigate whether the interfacial ferromagnetism stems from the intrinsic spin polarization of Ta $5d$ electrons at the KTaO_3 heterointerfaces, utilizing the element-specific technique and high sensitivity of XMCD. In Figure 4, we present the XMCD spectra near the Ta N_3 absorption edge for a representative $\text{LaAlO}_3/\text{KTaO}_3(111)$ sample at a temperature $T = 15$ K under an in-plane magnetic field. Remarkably, the

reproducible dichroism features appeared only near the absorption peaks (see Figure 4b) are discernable that resemble XMCD signals were observed at $\text{LaAlO}_3/\text{SrTiO}_3$ heterointerfaces⁵⁰, strongly indicating that these XMCD signals are indeed originating from the intrinsic spin polarization of the Ta $5d$ electrons. It is worth emphasizing that the magnetic behavior observed via Ta XMCD aligns with the SQUID measurements presented in Figure 2.

To further control our experiments, we also re-prepare and post-anneal the $\text{LaAlO}_3/\text{KTaO}_3(111)$ under various oxygen partial pressures (P_{O_2}) to effectively modulate the oxygen vacancies, thereby strengthening the theoretical scenario of emergent ferromagnetism induced by these vacancies, as illustrated in Figure 5. As expected from our intuitions, the increase in P_{O_2} gradually fills oxygen vacancies at the KTaO_3 heterointerfaces. This results in the enhancement of R_s (see Figure 5a) in the two-dimensional electron gases, accompanied by a substantial

reduction in both charge carrier density (see Figure 5b) and ferromagnetization (see Figure 5c,d). Notably, the magnetic response for the $\text{LaAlO}_3/\text{KTaO}_3$ post-annealed at a P_{O_2} of 1 mbar is significantly diminished, exhibiting an almost vanishing magnetic hysteresis loop (see Figure 5d). This underscores the pivotal role of oxygen vacancies in the emergence of interfacial ferromagnetism. Consequently, these independent and complementary electrical transport and magnetization measurements provide a robust and compelling evidence for that the ferromagnetic Ta at the superconducting KTaO_3 heterointerfaces is distinctly linked to the partially filled $5d$ electrons brought about by the oxygen vacancies.

Physically, since the conducting bands at the Fermi energy at the KTaO_3 heterointerfaces are predominantly Ta $5d$ orbitals, and the distinct ferromagnetism and superconductivity derive from the same Ta $5d$ electrons both theoretically and experimentally (see Figures 3 and 4), it is suggested that the superconductivity at the KTaO_3 heterointerfaces could spatially coexist with the ferromagnetism at low temperatures. In addition, a notable observation in Figure 2 is the two-dimensional superconductivity developed inside a ferromagnetic phase at the KTaO_3 heterointerfaces, implying that the ferromagnetism likely plays a crucial role in mediating the superconducting Cooper pairs⁴⁷. Significantly, the KTaO_3 heterointerfaces reveal mixed-parity superconductivity with an admixture of s -wave and p -wave pairings²⁴, compatible with the coexisting ferromagnetism. Moreover, it is intriguing that the KTaO_3 heterointerfaces exhibit the highest T_c of superconductivity among ferromagnetic EuO overlayer^{22,28}, suggesting that ferromagnetism may reinforce superconductivity. As a consequence, these complementary findings support the coexistence of ferromagnetism and superconductivity at the KTaO_3 heterointerfaces (see also Figure S14). The superconductivity observed at the KTaO_3 heterointerfaces is thus likely to be of nontrivial nature with broken time-reversal symmetry⁵¹, making it promising for potential applications in topological quantum computing⁵²⁻⁵⁵.

CONCLUSION

In summary, we have experimentally developed two-dimensional superconducting heterointerfaces of KTaO_3 and uncovered remarkable in-plane ferromagnetic hysteresis loops that persists above room temperature. Additionally, we conduct the first-principles calculations and XMCD measurements to elucidate further the intrinsic ferromagnetism emerging at the heterointerfaces of KTaO_3 . These intriguing findings highlight KTaO_3 heterointerfaces as time-reversal symmetry breaking superconductors. Our results therefore pave the way to further experimental and theoretical studies aimed at unraveling the intricate interplay among strong spin-orbit coupling, ferromagnetism, and superconductivity at the newly discovered KTaO_3 heterointerfaces.

Supporting Information

The Supporting Information is available free of charge at online.

Methods; Large-area AFM images of thin films and KTaO_3 substrates; XRD images of thin films and KTaO_3 substrates; Anisotropic superconductivity of $\text{LaAlO}_3/\text{KTaO}_3(111)$; Extrapolated BKT superconducting transition temperature; Temperature-dependent magnetization of KTaO_3 heterointerfaces; In-plane magnetization of KTaO_3 substrates; Out-of-plane magnetization of KTaO_3 substrates; XPS of KTaO_3 heterointerface and KTaO_3 substrate; SEM of KTaO_3 heterointerfaces; In-plane magnetization of $\text{LaAlO}_3/\text{KTaO}_3(111)$; In-plane magnetization of $\text{YAlO}_3/\text{KTaO}_3(111)$; Out-of-plane magnetization of $\text{LaAlO}_3/\text{KTaO}_3(111)$; Out-of-plane magnetization of $\text{YAlO}_3/\text{KTaO}_3(111)$; Field-dependent electrical characteristics of magnetization; High temperature-dependent in-plane magnetization for $\text{LaAlO}_3/\text{KTaO}_3(111)$; Electronic and magnetic properties of KTaO_3 heterointerfaces; Calculated PDOS of $(\text{LaAlO}_3)_6/(\text{KTaO}_3)_6(111)$ with an oxygen vacancy; Effective U_{eff} dependence of magnetic moments.

AUTHOR INFORMATION

*Corresponding Author

Shan Qiao, Email: qiaoshan@mail.sim.ac.cn

Gang Mu, Email: mugang@mail.sim.ac.cn

Yan Chen, Email: yanchen99@fudan.edu.cn

Wei Li, Email: w.li@fudan.edu.cn

Author Contributions

Z.N., J.Q., and Y.L. contributed equally to this work. W.L. and Y.C. conceived the project and designed the experiments. Z.N. and G.Z. grew the samples. Z.N., Y.L., F.C., G.Z., and G.M. performed the electrical transport measurements. Z.N. and Y.L. performed the magnetization measurements. M.Z., L.D., and S.Q. performed the XMCD measurement. X.Y. and Q.G. performed the XPS measurement. X.Y., Q.G., and H.J. performed the SEM measurement. W.P. and Y.C. assisted the magnetization, electrical transport and SEM experiments. J.Q. performed the first-principles calculations. W.L. wrote the paper with input from Z.N. and J.Q.. All authors discussed the results and gave approval to the final version of the manuscript.

Notes

The authors declare no competing financial interest.

Acknowledgements

This work is supported by the National Natural Science Foundation of China (Grant Nos. 11927807 and U2032207) and Shanghai Science and Technology Committee (Grant Nos. 23ZR1404600 and 20DZ1100604). The authors also thank beamline BL07U of the Shanghai Synchrotron Radiation Facility (SSRF).

- ¹ Mannhart, J.; Schlom, D. G. Oxide interfaces—An opportunity for electronics. *Science* **2010**, 327, 1607-1611.
- ² Zubko, P.; Gariglio, S.; Gabay, M.; Ghosez, P.; Triscone, J.-M. Interface physics in complex oxide heterostructures. *Annu. Rev. Condens. Matter Phys.* **2011**, 2, 141-165.
- ³ Hwang, H. Y.; Iwasa, Y.; Kawasaki, M.; Keimer, B.; Nagaosa, N.; Tokura, Y. Emergent phenomena at oxide interfaces. *Nat. Mater.* **2012**, 11, 103-113.
- ⁴ Huijben, M.; Brinkman, A.; Koster, G.; Rijnders, G.; Hilgenkamp, H.; Blank, D. H. A. Structure-property relation of SrTiO₃/LaAlO₃ interfaces. *Adv. Mater.* **2009**, 21, 1665-1677.
- ⁵ Ohtomo, A.; Hwang, H. Y. A high-mobility electron gas at the LaAlO₃/SrTiO₃ heterointerface. *Nature* **2004**, 427, 423-426.
- ⁶ Shalom, M. B.; Sachs, M.; Rakhmilevitch, D.; Palevski, A.; Dagan, Y. Tuning spin-orbit coupling and superconductivity at the SrTiO₃/LaAlO₃ interface: A magnetotransport study. *Phys. Rev. Lett.* **2010**, 104, 126802.
- ⁷ Caviglia, A. D.; Gabay, M.; Gariglio, S.; Reyren, N.; Cancellieri, C.; Triscone, J.-M. Tunable Rashba spin-orbit interaction at oxide interfaces. *Phys. Rev. Lett.* **2010**, 104, 126803.
- ⁸ Soumyanarayanan, A.; Reyren, N.; Fert, A.; Panagopoulos, C. Emergent phenomena induced by spin-orbit coupling at surfaces and interfaces. *Nature* **2016**, 539, 509-517.
- ⁹ Reyren, N.; Thiel, S.; Caviglia, A. D.; Kourkoutis, L. F.; Hammerl, G.; Richter, C.; Schneider, C. W.; Kopp, T.; Rüetschi, A.-S.; Jaccard, D.; Gabay, M.; Müller, D. A.; Triscone, J.-M.; Mannhart, J. Superconducting interfaces between insulating oxides. *Science* **2007**, 317, 1196-1199.
- ¹⁰ Caviglia, A. D.; Gariglio, S.; Reyren, N.; Jaccard, D.; Schneider, T.; Gabay, M.; Thiel, S.; Hammerl, G.; Mannhart, J.; Triscone, J.-M. Electric field control of the LaAlO₃/SrTiO₃ interface ground state. *Nature* **2008**, 456, 624-627.
- ¹¹ Brinkman, A.; Huijben, M.; Zalk, M. van; Huijben, J.; Zeitler, U.; Maan, J. C.; Wiel, W. G. van der; Rijnders, G.; Blank, D. H. A.; Hilgenkamp, H. Magnetic effects at the interface between non-magnetic oxides. *Nat. Mater.* **2007**, 6, 493-496.
- ¹² Ariando; Wang, X.; Baskaran, G.; Liu, Z. Q.; Huijben, J.; Yi, J. B.; Annadi, A.; Barman, A. R.; Rusydi, A.; Dhar, S.; Feng, Y. P.; Ding, J.; Hilgenkamp, H.; Venkatesan, T. Electronic phase separation at the LaAlO₃/SrTiO₃ interface. *Nat. Commun.* **2011**, 2, 188.
- ¹³ Li, L.; Richter, C.; Mannhart, J.; Ashoori, R. C. Coexistence of magnetic order and two-dimensional superconductivity at LaAlO₃/SrTiO₃ interfaces. *Nat. Phys.* **2011**, 7, 762-766.
- ¹⁴ Bert, J. A.; Kalisky, B.; Bell, C.; Kim, M.; Hikita, Y.; Hwang, H. Y.; Moler, K. A. Direct imaging of the coexistence of ferromagnetism and superconductivity at the LaAlO₃/SrTiO₃ interface. *Nat. Phys.* **2011**, 7, 767-771.
- ¹⁵ Dikin, D. A.; Mehta, M.; Bark, C. W.; Folkman, C. M.; Eom, C. B.; Chandrasekhar, V. Coexistence of superconductivity and ferromagnetism in two dimensions. *Phys. Rev. Lett.* **2011**, 107, 056802.
- ¹⁶ Michaeli, K.; Potter, A. C.; Lee, P. A. Superconducting and ferromagnetic phases in SrTiO₃/LaAlO₃ oxide interface structures: Possibility of finite momentum pairing. *Phys. Rev. Lett.* **2012**, 108, 117003.
- ¹⁷ Kozii, V.; Fu, L. Odd-parity superconductivity in the vicinity of inversion symmetry breaking in spin-orbit-coupled systems. *Phys. Rev. Lett.* **2015**, 115, 207002.
- ¹⁸ Nakosai, S.; Tanaka, Y.; Nagaosa, N. Topological superconductivity in bilayer Rashba system. *Phys. Rev. Lett.* **2012**, 108, 147003.
- ¹⁹ Potter, A. C.; Lee, P. A. Engineering a $p+ip$ superconductor: Comparison of topological insulator and Rashba spin-orbit-coupled materials. *Phys. Rev. B* **2011**, 83, 184520.
- ²⁰ Fitzsimmons, M. R.; Hengartner, N. W.; Singh, S.; Zhermenkov, M.; Bruno, F. Y.; Santamaria, J.; Brinkman, A.; Huijben, M.; Molegraaf, H. J. A.; Venta, J. de la; Schuller, I. K. Upper limit to magnetism in LaAlO₃/SrTiO₃ heterostructures. *Phys. Rev. Lett.* **2011**, 107, 217201.
- ²¹ Salman, Z.; Ofer, O.; Radovic, M.; Hao, H.; Shalom, M. B.; Chow, K. H.; Dagan, Y.; Hossain, M. D.; Levy, C. D. P.; MacFarlane, W. A.; Morris, G. M.; Patthey, L.; Pearson, M. R.; Saadaoui, H.; Schmitt, T.; Wang, D.; Kiefl, R. F. Nature of weak magnetism in SrTiO₃/LaAlO₃ multilayers. *Phys. Rev. Lett.* **2012**, 109, 257207.
- ²² Liu, C.; Yan, X.; Jin, D.; Ma, Y.; Hsiao, H.-W.; Lin, Y.; Bretz-Sullivan, T. M.; Zhou, X.; Pearson, J.; Fisher, B.; Jiang, J. S.; Han, W.; Zuo, J.-M.; Wen, J.; Fong, D. D.; Sun, J.; Zhou, H.; Bhattacharya, A. Two-dimensional superconductivity and anisotropic transport at KTaO₃ (111) interfaces. *Science* **2021**, 371, 716-721.
- ²³ Chen, Z.; Liu, Z.; Sun, Y.; Chen, X.; Liu, Y.; Zhang, H.; Li, H.; Zhang, M.; Hong, S.; Ren, T.; Zhang, C.; Tian, H.; Zhou, Y.; Sun, J.; Xie, Y. Two-dimensional superconductivity at the LaAlO₃/KTaO₃(110) heterointerface. *Phys. Rev. Lett.* **2021**, 126, 026802.
- ²⁴ Zhang, G.; Wang, L.; Wang, J.; Li, G.; Huang, G.; Yang, G.; Xue, H.; Ning, Z.; Wu, Y.; Xu, J.-P.; Song, Y.; An, Z.; Zheng, C.; Shen, J.; Li, J.; Chen, Y.; Li, W. Spontaneous rotational symmetry breaking in KTaO₃ interface superconductor. *Nat. Commun.* **2023**, 14, 3046.
- ²⁵ Ueno, K.; Nakamura, S.; Shimotani, H.; Yuan, H. T.; Kimura, N.; Nojima, T.; Aoki, H.; Iwasa, Y.; Kawasaki, M. Discovery of superconductivity in KTaO₃ by electrostatic carrier doping. *Nat. Nanotechnol.* **2011**, 6, 408-412.
- ²⁶ Bruno, F. Y.; Walker, S. M.; Riccò, S.; Torre, A. de la; Wang, Z.; Tamai, A.; Kim, T. K.; Hoesch, M.; Bahramy, M. S.; Baumberger, F. Band structure and spin-orbital texture of the (111)-KTaO₃ 2D electron gas. *Adv. Electron. Mater.* **2019**, 5, 1800860.
- ²⁷ Mallik, S.; Ménard, G. C.; Saiz, G.; Witt, H.; Lesueur, J.; Gloter, A.; Benfatto, L.; Bibes, M.; Bergeal, N. Superfluid stiffness of a KTaO₃-based two-dimensional electron gas. *Nat. Commun.* **2022**, 13, 4625.
- ²⁸ Hua, X.; Meng, F.; Huang, Z.; Li, Z.; Wang, S.; Ge, B.; Xiang, Z.; Chen, X. Tunable two-dimensional superconductivity and spin-orbit coupling at the EuO/KTaO₃(110) interface. *npj Quantum Mater.* **2022**, 7, 97.
- ²⁹ Arnault, E. G.; Al-Tawhid, A. H.; Salmani-Rezaie, S.; Müller, D. A.; Kumah, D. P.; Bahramy, M. S.; Finkelstein, G.; Ahadi, K. Anisotropic superconductivity at KTaO₃(111) interfaces. *Sci. Adv.* **2023**, 9, eadf1414.
- ³⁰ Al-Tawhid, A. H.; Poage, S. J.; Salmani-Rezaie, S.; Gonzalez, A.; Chikara, S.; Müller, D. A.; Kumah, D. P.; Gas-

- tiasoro, M. N.; Lorenzana, J.; Ahadi, K. Enhanced critical field of superconductivity at an oxide interface. *Nano Lett.* **2023**, *23*, 6944-6950.
- ³¹ Al-Tawhid, A. H.; Kanter, J.; Hatefipour, M.; Irving, D. L.; Kumah, D. P.; Shabani, J.; Ahadi, K. Oxygen vacancy-induced anomalous Hall effect in a nominally non-magnetic oxide. *J. Electron. Mater.* **2022**, *51*, 7073-7077.
- ³² Krantz, P. W.; Tyner, A.; Goswami, P.; Chandrasekhar, V. Intrinsic magnetism in KTaO₃ heterostructures. *Appl. Phys. Lett.* **2024**, *124*, 093102.
- ³³ Jiang, D.; Yuan, T.; Wu, Y.; Wei, X.; Mu, G.; An, Z.; Li, W. Strong in-plane magnetic field induced reemergent superconductivity in the van der Waals heterointerface of NbSe₂ and CrCl₃. *ACS Appl. Mater. Interfaces* **2020**, *12*, 49252-49257.
- ³⁴ Zou, M.; Chu, J.; Zhang, H.; Yuan, T.; Cheng, P.; Jin, W.; Jiang, D.; Xu, X.; Yu, W.; An, Z.; Wei, X.; Mu, G.; Li, W. Evidence for ferromagnetic order in the CoSb layer of LaCoSb₂. *Phys. Rev. B* **2020**, *101*, 155138.
- ³⁵ Xue, H.; Wang, L.; Wang, Z.; Zhang, G.; Peng, W.; Wu, S.; Gao, C.-L.; An, Z.; Chen, Y.; Li, W. Fourfold symmetric superconductivity in spinel oxide LiTi₂O₄(001) thin films. *ACS Nano* **2022**, *16*, 19464-19471.
- ³⁶ Tinkham, M. Effect of fluxoid quantization on transitions of superconducting films. *Phys. Rev.* **1963**, *129*, 2413-2422.
- ³⁷ Wang, L.; He, W.; Huang, G.; Xue, H.; Zhang, G.; Mu, G.; Wu, S.; An, Z.; Zheng, C.; Chen, Y.; Li, W. Two-dimensional superconductivity at the titanium sesquioxide heterointerface. *ACS Nano* **2022**, *16*, 16150-16157.
- ³⁸ Zhang, G.; Liu, Y.; Li, G.; Wang, J.; Wu, Y.; Wang, L.; Xue, H.; Ning, Z.; Gao, C.; An, Z.; Li, J.; Shen, J.; Mu, G.; Chen, Y.; Li, W. Quantum metallic state in the titanium sesquioxide heterointerface superconductor. arXiv:2211.04035 (2022).
- ³⁹ Lu, J. M.; Zheliuk, O.; Leermakers, I.; Yuan, N. F. Q.; Zeitler, U.; Law, K. T.; Ye, J. T. Evidence for two-dimensional Ising superconductivity in gated MoS₂. *Science* **2015**, *350*, 1353-1357.
- ⁴⁰ Kosterlitz, J. M.; Thouless, D. J. Long range order and metastability in two dimensional solids and superfluids. *J. Phys.: Condens. Matter* **1972**, *5*, L124-L126.
- ⁴¹ Beasley, M. R.; Mooij, J. E.; Orlando, T. P. Possibility of vortex-antivortex pair dissociation in two-dimensional superconductors. *Phys. Rev. Lett.* **1979**, *42*, 1165-1168.
- ⁴² Halperin, B. I.; Nelson, D. R. Resistive transition in superconducting films. *J. Low Temp. Phys.* **1979**, *36*, 599-616.
- ⁴³ Zhang, H.; Yun, Y.; Zhang, X.; Zhang, H.; Ma, Y.; Yan, X.; Wang, F.; Li, G.; Li, R.; Khan, T.; Chen, Y.; Liu, W.; Hu, F.; Liu, B.; Shen, B.; Han, W.; Sun, J. High-mobility spin-polarized two-dimensional electron gases at EuO/KTaO₃ interfaces. *Phys. Rev. Lett.* **2018**, *121*, 116803.
- ⁴⁴ Hua, X.; Zeng, Z.; Meng, F.; Yao, H.; Huang, Z.; Long, X.; Li, Z.; Wang, Y.; Wang, Z.; Wu, T.; Weng, Z.; Wang, Y.; Liu, Z.; Xiang, Z.; Chen, X. Superconducting stripes induced by ferromagnetic proximity in an oxide heterostructure. *Nat. Phys.* **2024**.
- ⁴⁵ Bonilla, M.; Kolekar, S.; Ma, Y.; Diaz, H. C.; Kalappattil, V.; Das, R.; Eggers, T.; Gutierrez, H. R.; Phan, M.-H.; Batzill, M. Strong room-temperature ferromagnetism in VSe₂ monolayers on van der Waals substrates. *Nat. Nanotechnol.* **2018**, *13*, 289-293.
- ⁴⁶ Pfeleiderer, C. Superconducting phases of *f*-electron compounds. *Rev. Mod. Phys.* **2009**, *81*, 1551-1624.
- ⁴⁷ Ghosh, S. K.; Smidman, M.; Shang, T.; Annett, J. F.; Hillier, A. D.; Quintanilla, J.; Yuan, H. Recent progress on superconductors with time-reversal symmetry breaking. *J. Phys.: Condens. Matter* **2021**, *33*, 033001.
- ⁴⁸ Fujii, Y.; Sakudo, T. Dielectric and optical properties of KTaO₃. *J. Phys. Soc. Jpn.* **1976**, *41*, 888-893.
- ⁴⁹ Pentcheva, R.; Pickett, W. E. Correlation-driven charge order at the interface between a Mott and a band insulator. *Phys. Rev. Lett.* **2007**, *99*, 016802.
- ⁵⁰ Lee, J.-S.; Xie, Y. W.; Sato, H. K.; Bell, C.; Hikita, Y.; Hwang, H. Y.; Kao, C.-C. Titanium *d_{xy}* ferromagnetism at the LaAlO₃/SrTiO₃ interface. *Nat. Mater.* **2013**, *12*, 703-706.
- ⁵¹ Stewart, G. R. Unconventional superconductivity. *Adv. Phys.* **2017**, *66*, 75-196.
- ⁵² Nayak, C.; Simon, S. H.; Stern, A.; Freedman, M.; Sarma, S. D. Non-Abelian anyons and topological quantum computation. *Rev. Mod. Phys.* **2008**, *80*, 1083-1159.
- ⁵³ Alicea, J. New directions in the pursuit of Majorana fermions in solid state systems. *Rep. Prog. Phys.* **2012**, *75*, 076501.
- ⁵⁴ Beenakker, C. W. J. Search for Majorana fermions in superconductors. *Annu. Rev. Condens. Matter Phys.* **2013**, *4*, 113-136.
- ⁵⁵ Elliott, S. R.; Franz, M. Majorana fermions in nuclear, particle, and solid-state physics. *Rev. Mod. Phys.* **2015**, *87*, 137-163.